Bulletin of the Institute of Earth Sciences, Academia Sinica, Vol. 1, PP. 111 – 126, December 1981

SURFACE WAVE DISPERSION AND CRUST-MANTLE STRUCTURE IN THE SOUTHWEST PACIFIC

by Yeong Tein Yeh and Kou Cheng Chen

ABSTRACT

The display-equalized filter was used to measure group velocity dispersion for both Rayleigh and Love waves from 26 earthquakes located in Tonga, Kermadec, and New Britain areas. The propagation paths for these events can be divided into two sets: (1) Tonga to Taipei, and (2) Kermadec and New Britain to Taipei. The resulting dispersion curves were then grouped and each velocity data set was inverted using extended Backus-Gilbert inversion method. The resulting regional structures for the two paths show only some differences at a depth shallower than 75 km.

INTRODUCTION

It is well known that surface wave group velocity dispersion observations can be inverted to obtain the average structure between earthquake epicenters and recording stations. Because of the difficulties in applying other geophysical methods, surface wave data interpretations of Earth structure is particularly useful for remote area, such as the oceanic region. Most of the earlier studies for surface wave velocity characteristics in the southwest Pacific have concentrated on Rayleigh wave measurements in the period range of 20-140 seconds (Kuo et al., 1962; Santo and Sato, 1966; Savage and White, 1969; Gupta and Hamada, 1975; Seneff, 1977). Gupta and Hamada (1975) also obtained Love wave dispersion in the 30- to 40-sec period range for paths in this region.

Recently, the improvements of the filtering techniques for analyzing seismic records and the installation of high quality Seismic Research Observatories (SRO) made it possible to estimate dispersion data for longer period. In the present paper we have investigated Rayleigh and Love wave dispersion characteristics for 26 paths in the southwest Pacific region, from Tonga, Kermadec, and New Britain to Taiwan, in the period range of about 20-300 seconds. The extended Backus-Gilbert method was used to invert the obtained data for crust and upper mantle structures in this area.

REGIONAL TECTONICS

The region of the southwest Pacific considered in present research is tectonically complex and interesting (Figure 1). It includes part of the Philippine Sea plate and the boundary area of the Pacific and the Australian plates. The major tectonic elements in the boundary area, from east to west, are the Tonga-Kermadec trench and ridge, the Fiji basin, the New Hebrides islands and trench, the Solomon islands and trench, the Ontong-Java plateau, and the Caroline basin and islands (Figure 1a).

The Australian plate underthrusts the Pacific plate to the NNE under east along the Tonga-Kermadec arc. The convergence of these two plates in northwestern New Guinea is along NNE-SSW direction. The relative motions of the plates near the Bismark Archipelago are complex because of the presence of at least three additional small plates (Figure 1b; Johnson and Molnar, 1972).

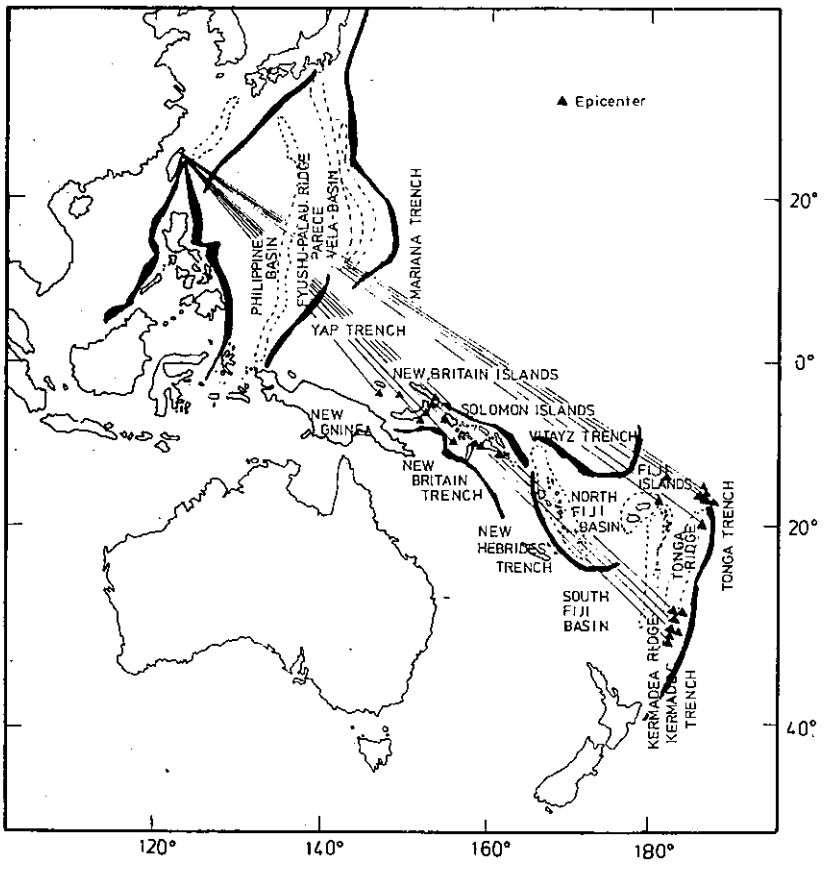

Figure 1a. Major tectonic elements of the southwest Pacific and propagation paths for the earthquakes selected.

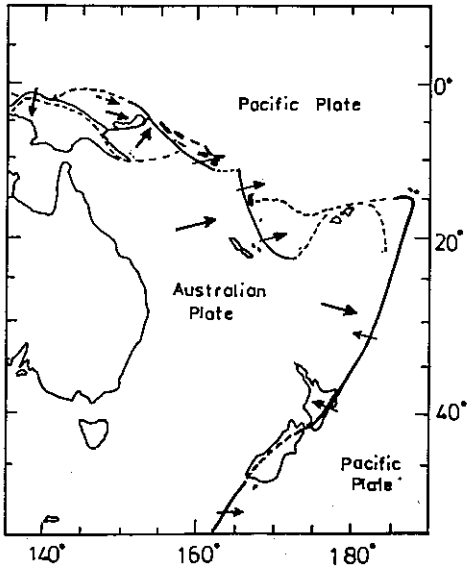

Figure 1b. Plate motions in the southwest Pacific (from Johnson and Molnar, 1972)

The portion of the Philippine Sea plate studied here is from south of the Mariana trench and the Yap trench to Taiwan (Figure 1a). It includes the Parece Vela and the Philippine basins and the Kyushu ridge.

The current direction of relative motion of the Philippine Sea plate with respect to the Eurasian plate in Taiwan region is about northwest (Seno, 1977; Lin and Tsai, 1980). The convergence of the Pacific and the Philippine Sea plates is in E-W direction (Isacks, et al., 1968).

Karig (1970, 1971a, b) has proposed that an extensional origin for crust in a region, called an active marginal basin, behind the island arcs, including the Tonga, Kermadec, Mariana, and New Hebrides systems. This basin is bounded by scarps and contains abundant normal faults with associated rough topograph. Sediments are thin and heat flow is high in the active marginal basin.

DATA SELECTION AND ANALYSIS

The monthly listing of Preliminary Determination of Epicenters (PDE Monthly) was used to find the events located in the vicinity of the Tonga, Kermadec, and New Britain islands. The analog recordings from Seismic Research Observatory (SRO) in Taipei, Taiwan were first examined to confirm the record quality of the earthquakes selected. For an event to be accepted for analysis, it was required that the seismic signal be easily identified visually and have a high signal to noise ratio. Table 1 lists the pertinent hypocentral information and origin times of earthquakes finally selected for this research; the locations of these events and their propagation paths are shown in Figure 1a. The first column in Table 1 shows the reference code with which we can distinguish the group of earthquakes that have similar propagation paths. After time windows of the chosen seismograms were determined, the digital recordings were played back for analysis.

The Taipei SRO station, located at 121.489°E and 24.976°N, is a newly installed high quality seismic system which can produce both analog and digital data. The seismometer of this system is situated at a depth of about 100 meters to reduce long period noise. Digital sensitivity for the long period data is set to 5000 digital counts per micron of ground displacement at 25 seconds period. The sampling rate is one sample per second.

The display-equalized filtering technique (Nyman and Landisman, 1977) was used to analyze digital data for group velocity dispersion curves. The method is a modified form of the multiple band-pass filter (Dziwonski et al., 1969). A brief review of the method is given below.

Let $x(t)$ and $A(\omega, t)$ represent the seismic signal and its component at frequency ω respectively. In the time domain, A is estimated from the convolution of $x(t)$ with a filter $h_\omega(t)$. That is

$$A(\omega, t) = \int_{-\infty}^{\infty} x(\tau)\, h_\omega(t-\tau)\, d\tau \tag{1}$$

where

$$h_\omega(t) = (4\pi\alpha)^{-1/2} \exp(-t^2/4\alpha) \exp(i\omega t). \tag{2}$$

Conventionally, the results of filtering are displayed as a two-dimensional array of amplitude values. Consective rows correspond to equal increments in group velocity, while consecutive columns correspond to equal increments in log period. Levels of constant amplitude are often contoured to assist the interpretation of the observed dispersed patterns.

Table 1
Hypocenter data

Ref. Code	Date	Origin Time (GMT)	Lat. (deg)	Long. (deg)	Depth (km)	Mag. (m_b)
BRI 1	07-23-76	16-45-43.6	3.508S	148.647E	37	5.3
BRI 2	07-29-77	11-15-45.3	8.031S	155.538E	33	6.4
BRI 3	08-08-77	12-58-45.0	10.567S	161.333E	32	5.8
BRI 4	08-12-77	00-07-51.8	6.533S	155.011E	58	5.9
BRI 5	01-20-78	00-24-26.4	9.790S	159.475E	73	5.5
BRI 6	01-25-78	23-18-56.6	5.339S	151.676E	44	6.1
BRI 7	01-29-78	14-17-30.1	4.224S	152.808E	20	5.7
BRI 8	02-02-78	07-58-05.6	5.531S	151.675E	33	5.6
BRI 9	03-04-78	14-58-13.0	4.656S	153.101E	78	6.2
BRI10	11-21-78	11-03-42.3	3.268S	146.911E	33	5.6
BRI11	11-06-79	11-38-31.5	9.498S	159.220E	30	6.0
KER 1	07-31-76	00-46-58.0	30.322S	177.964W	20	5.8
KER 2	08-28-77	14-11-30.3	29.062S	177.148W	44	5.5
KER 3	10-05-77	10-27-46.3	29.011S	176.894W	56	5.4
KER 4	01-14-78	15-20-54.2	30.115S	177.489W	44	5.8
KER 5	01-15-78	06-56-34.5	30.209S	177.554W	17	5.6
KER 6	01-30-78	06-51-13.6	29.780S	177.220W	39	5.6
KER 7	02-11-78	20-05-23.0	30.414S	177.119W	33	5.5
TON 1	07-24-77	06-22-51.3	15.339S	173.152W	33	6.0
TON 2	09-13-77	00-21-52.6	15.454S	173.289W	33	5.7
TON 3	10-14-77	04-55-34.8	15.723S	173.046W	33	5.9
TON 4	10-26-77	11-20-16.1	15.550S	177.395W	41	5.0
TON 5	06-17-77	15-11-33.5	17.098S	172.264W	33	6.6
TON 6	07-27-78	18-25-08.5	15.584S	173.043W	33	5.7
TON 7	11-16-79	15-21-25.7	16.760S	179.984W	33	6.1
TON 8	04-30-80	11-37-06.8	19.428S	173.906W	33	5.6

In the display-equalized filter, the parameter α in (2) is defined at each period and velocity such that the widths of the filter in the frequency and in the time domain span an optimum number of columns and rows, respectively, in the display. In this sense, the local value of α is

$$\alpha = \frac{\epsilon \Delta dv T_j}{4\pi \xi v_k^2} \tag{3}$$

where

Δ = epicentral distance,
dv = group velocity increment,
T_j = period for column j,

$$\xi = \frac{T_j + 1}{T_j} - 1$$

and

ϵ = the ellipticity parameter.

The amplitude value A_{jk} determined from (1) at each grid point represents an average over some region in the 'group velocity/log-period plane'. The parameter ϵ is directly related to the ellipticity of the averaging region.

In order to understand the advantages and disadvantages of the conventional multiple and the display-equalized filters, both the methods have been tested by using synthetic seismograms. The results show that sometimes, the errors introduced by the display-equalized filter may be larger than those introduced by the multiple filter. The display-equalized filter often gives more stable and broad period range dispersion measurements. The test also shows that a value of 2 for ϵ may be proper. Figure 2 shows one of the testing results. The largest measuring error for the display-equalized filter is about 0.06 km/sec.

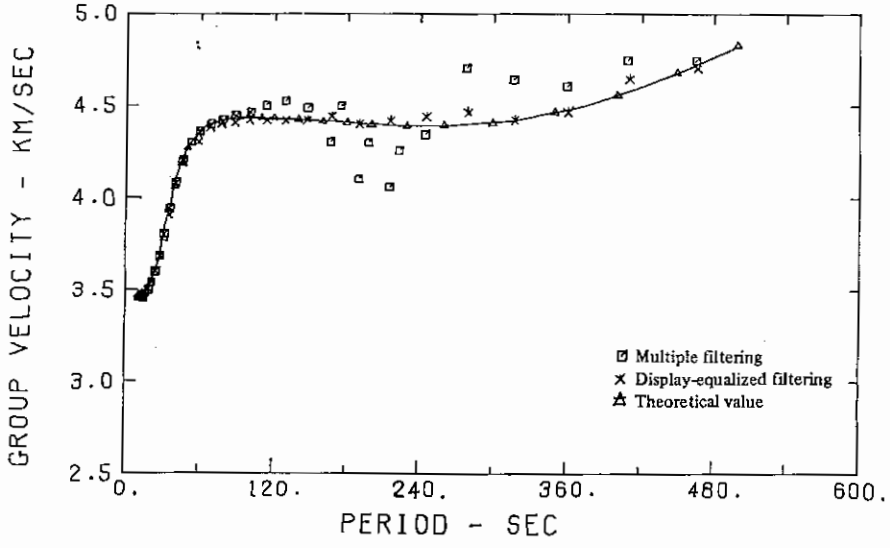

Figure 2. Results of theoretical test for the multiple filter and the display-equalized filter for ϵ=2.

After testing, the method was used to analyze the selected data. In this research, Rayleigh wave dispersion was determined from the vertical component seismograms. Seismograms for north-south and east-west directions were rotated to obtain the Love component. The radial motion was also analyzed for reference. In the analysis, instrumental group delay was corrected by using the formula

$$t_g = \frac{1}{0.0155+0.1968\omega-0.3866\omega^2+0.9988\omega^3-0.8518\omega^4} \tag{4}$$

developed, for SRO long period system, by McCowan and Lacoss (1978). The largest error introduced by (4) is about 1.25 seconds, for periods longer than 150 seconds, which is negligible compared to our travel time.

EXPERIMENTAL RESULTS

Figures 3 to 5 present the measured dispersion data for the three groups of propagation paths, i.e., the Tonga islands to Taipei, the Kermadec islands to Taipei, and the New Britain area to Taipei, respectively. The period range covered, both for Rayleigh and Love waves, are approximately 20-300 seconds.

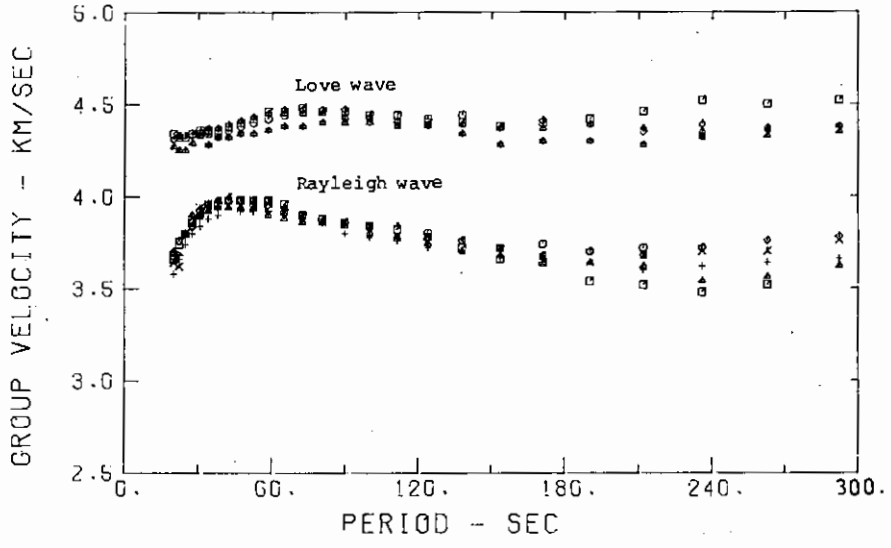

Figure 3. Measured group velocities for the path Tonga-Taipei.

The scatter in the group velocity dispersion measurements may be caused by a number of factors, such as errors in event location and origin time, noise contamination, neglect of the correction for source group delay, structural variations along the different propagation paths, and errors introduced by data processing. However, despite the scatter the distinctive features of the dispersion curves are clear and consistent.

The signals generated by earthquakes of the Kermadec group travel across the boundary area of the Pacific and the Australian plates and the south Philippine Sea plate (Figure 1a). The great circle paths for events of the New Britain group are somewhat coincided with part of those for the Kermadec group. Indeed, the resulting dispersion curves for these two groups are very similar (compare Figures 4 with 5). This may suggest that the average structure along the propagation path Kermadec-Taipei is about the same as that along the propagation path New Britain-

Taipei. Accordingly, we computed the average dispersion curves and the standard deviations for these two paths (Figure 6 and Table 2). The maximum standard error for this data set is approximately 0.08 km/sec. The results were then used to invert for the average crust-mantle structure.

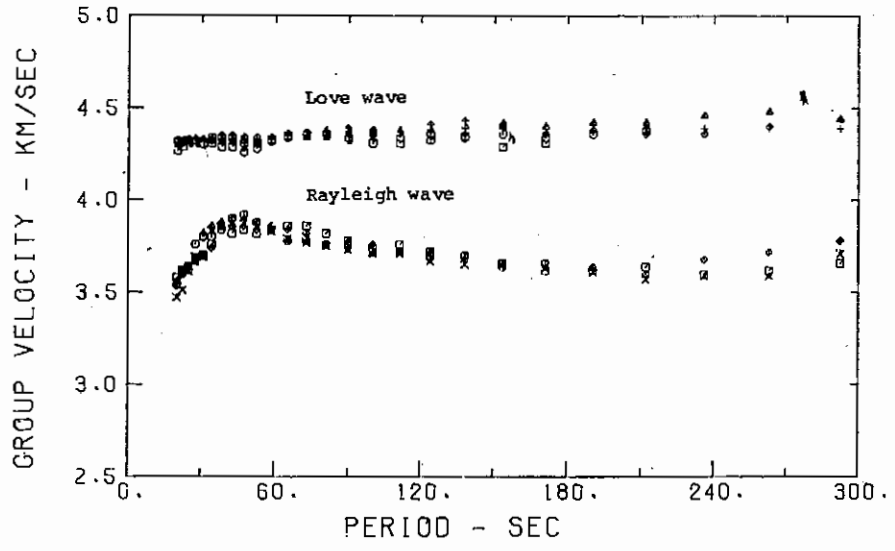

Figure 4. Measured group velocities for the path Kermadec-Taipei.

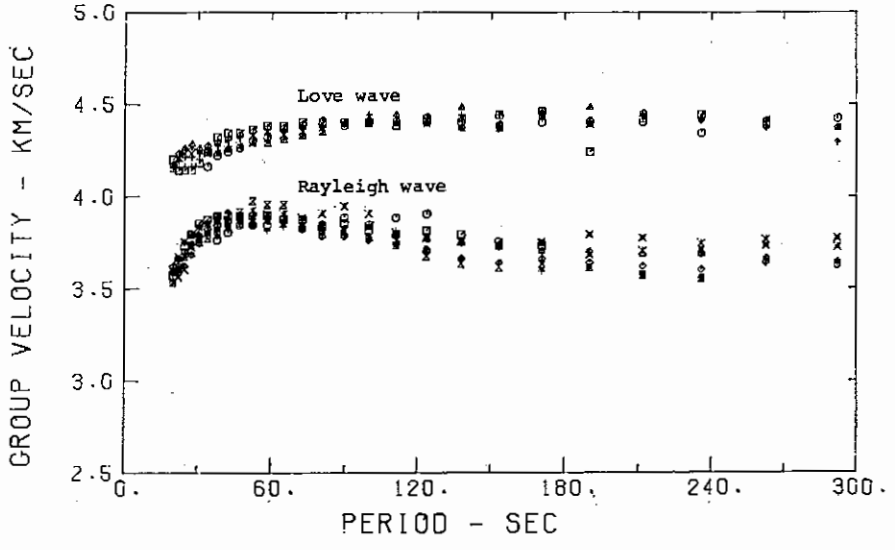

Figure 5. Measured group velocities for the path New Britain-Taipei.

Earthquakes of the Tonga group propagate to the SRO station in Taipei mostly along the paths confined to the boundary of the Pacific plate and the Philippine Sea plate (Figure 1a). The measured dispersion data are averaged and shown in Figure 7 and Table 2. The standard deviations are also presented. The maximum standard error for this data set is about 0.1 km/sec. Compare Figures 6 with 7, we can see that the differences between these two data sets are, mainly, in short period

Table 2
Average group velocities and standard deviations

	Period (sec)	BRI-KER LR (km/sec)	STD (km/sec)	BRI-KER LQ (km/sec)	STD (km/sec)	Tonga LR (km/sec)	STD (km/sec)	Tonga LQ (km/sec)	STD (km/sec)
1	292.4000	3.7000	0.0620	4.3890	0.0530	3.7050	0.0770	4.4170	0.0910
2	262.7000	3.6690	0.0610	4.4050	0.0330	3.6360	0.0980	4.3900	0.0750
3	235.9000	3.6330	0.0700	4.4050	0.0400	3.6300	0.1020	4.3950	0.0880
4	211.9000	3.6360	0.0700	4.4090	0.0280	3.6360	0.0720	4.3650	0.0740
5	190.4000	3.6560	0.0600	4.3840	0.0610	3.6430	0.0590	4.3750	0.0520
6	171.0000	3.6700	0.0530	4.4040	0.0500	3.6730	0.0370	4.3700	0.0500
7	153.6000	3.6730	0.0480	4.3860	0.0390	3.6940	0.0280	4.3560	0.0430
8	138.0000	3.7010	0.0500	4.3970	0.0400	3.7290	0.0300	4.3920	0.0360
9	123.9000	3.7380	0.0660	4.3880	0.0320	3.7630	0.0290	4.3960	0.0150
10	111.3000	3.7610	0.0480	4.3780	0.0330	3.7970	0.0290	4.4160	0.0250
11	100.0000	3.7800	0.0530	4.3800	0.0330	3.7970	0.0290	4.4160	0.0250
12	89.8300	3.8040	0.0540	4.3770	0.0240	3.8490	0.0230	4.4440	0.0290
13	80.6900	3.8050	0.0430	4.3720	0.0210	3.8690	0.0110	4.4480	0.0280
14	72.4800	3.8310	0.0360	4.3630	0.0200	3.8990	0.0160	4.4480	0.0400
15	65.1000	3.8510	0.0440	4.3490	0.0210	3.9200	0.0260	4.4400	0.0350
16	58.4800	3.8640	0.0350	4.3320	0.0250	3.9460	0.0320	4.4280	0.0410
17	52.5300	3.8760	0.0380	4.3140	0.0260	3.9570	0.0240	4.4040	0.0380
18	47.1900	3.8760	0.0250	4.3020	0.0310	3.9600	0.0260	4.3880	0.0290
19	42.3900	3.8610	0.0340	4.3020	0.0360	3.9660	0.0250	4.3640	0.0270
20	38.0700	3.8400	0.0370	4.2880	0.0420	3.9510	0.0280	4.3520	0.0220
21	34.2000	3.8130	0.0410	4.2700	0.0530	3.9370	0.0290	4.3400	0.0350
22	30.7200	3.7740	0.0520	4.2710	0.0550	3.9000	0.0330	4.3450	0.0130
23	27.5900	3.7270	0.0450	4.2650	0.0720	3.8510	0.0320	4.3250	0.0240
24	24.7900	3.6670	0.0510	4.2630	0.0720	3.7870	0.0240	4.3050	0.0370
25	22.2700	3.6100	0.0430	4.2490	0.0700	3.7030	0.0590	4.3050	0.0370
26	20.000	3.5580	0.0380	4.2350	0.0780	3.6530	0.0410	4.3150	0.0330

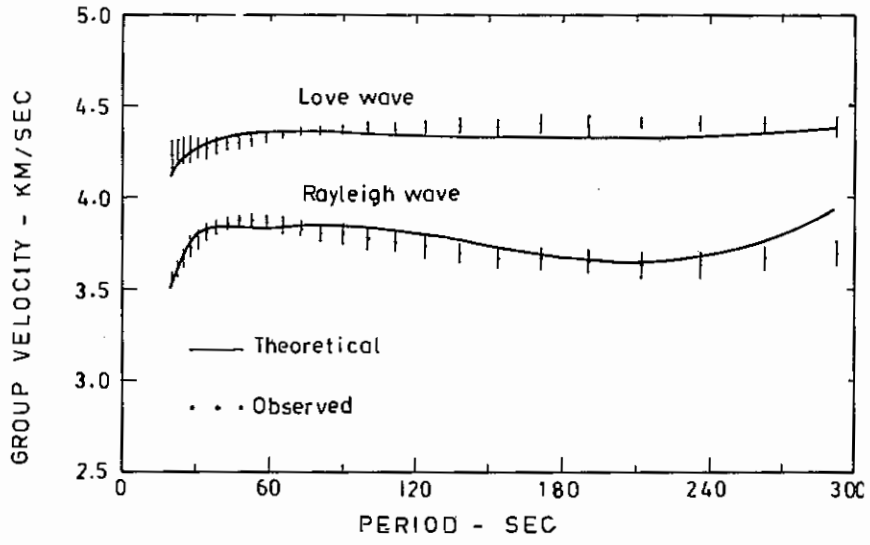

Figure 6. Theoretical and observed group velocities and corresponding error bars for the Kermadec-New Britain-Taipei model KNB.

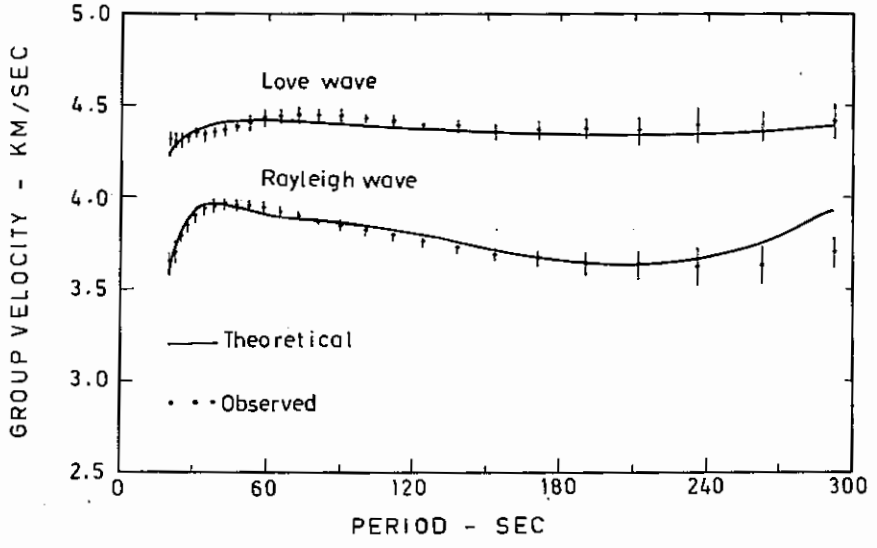

Figure 7. Theoretical and observed group velocities and corresponding error bars for the Tonga-Taipei model TON.

range. This may indicate that the lateral structure variations in the Tonga-Kermadec-Taiwan area are limited to the shallow depth.

INVERSION METHOD

The general equation for geophysical inverse problem can be written in the form

$$\Delta D = A\Delta P + N, \tag{5}$$

where ΔD is an m by 1 matrix representing the difference between the observations and the theoretical values, A is an m by n matrix of first order partial derivatives,

ΔP is an n by 1 matrix consisting of the unknown parameter corrections, and N is an m by 1 vector denoting the observational error (Franklin, 1970; Jordon, 1973; Rodi, 1975; Yeh, 1979). For application to surface wave studies, Earth structure is assumed to be layered and our interest is to determine the physical properties of each layer. Therefore, a δ-ness vector, $X^T = (0,0,...,1,0,0,...0)$ can be used to specified the parameter elements, i.e.

$$X^T \Delta P = \Delta p_i \tag{6}$$

Assuming that ΔD, ΔP, and N are zero mean random variables and the variance matrices of ΔP and N are

$$\text{var}(\Delta P) = W$$

and

$$\text{var}(N) = E,$$

respectively. The best unbiased estimate $\overline{\Delta p_i}$ of Δp_i is

$$\overline{\Delta p_i} = X^T W A^T (AWA^T + E)^{-1} \Delta D \tag{7}$$

and its variance is

$$\sigma^2 = X^T W X - X^T W A^T (AWA^T + E)^{-1} AWX \tag{8}$$

(Rodi, 1975; Yeh, 1979). In deriving (8) and (9) we also suppose that ΔP and N are uncorrelated and W and E are positive definite.

For $\overline{\Delta p_i}$ to be meaningful we must be able to measure how successfully it approximates the desired solution Δp_i. Substituting (5) into (7) and using (6) we obtain,

$$e = (A^T L - X)^T \Delta P + L^T N, \tag{9}$$

the error of the estimate, where

$$L = (AWA^T + E)^{-1} AWX. \tag{10}$$

The error e has two terms, one due to $A^T L \neq X$ and the other due to noise N. If we define the averaging kernel K as follows,

$$K = A^T L, \tag{11}$$

then, clearly the shape of K is an indication of how well the estimated $\overline{\Delta p_i}$ resembling the desired solution Δp_i. A quantitative evaluation can be achieved by using the 'relative success' parameter s^2, where

$$s^2 = 1 - \frac{\delta^2}{\sigma_0^2} \tag{12}$$

with

$$\delta^2 = (X-K)^T W (X-K) \tag{13}$$

and

$$\sigma_0^2 = X^T W X. \tag{14}$$

Table 3.
Layer shear velocities and resolution parameters for model KNB

H (km)	β (km/sec)	σ (km/sec)	s^2
2.5	0.000	0.000	0.000
1.5	1.306	0.162	0.022
3.0	3.385	0.109	0.156
5.0	3.883	0.076	0.373
5.0	4.379	0.080	0.262
10.0	4.258	0.052	0.385
10.0	4.582	0.055	0.275
10.0	4.469	0.056	0.267
15.0	4.474	0.043	0.384
15.0	4.525	0.045	0.259
15.0	4.336	0.047	0.220
15.0	4.341	0.048	0.180
20.0	4.349	0.041	0.197
30.0	4.580	0.033	0.216
40.0	4.595	0.029	0.210
40.0	4.590	0.030	0.152
40.0	4.563	0.030	0.110
50.0	4.520	0.027	0.096
50.0	4.476	0.027	0.069
50.0	5.390	0.028	0.027
100.0	5.371	0.019	0.033
100.0	5.372	0.019	0.016
150.0	5.884	0.016	0.008
∞	6.380		

Because δ^2 is a natural definition for the farness of K from X, and σ_0^2 is a measure of the size of X, s^2 is a normalized measurement of the 'successfulness' of K as an approximation to X. It can be shown that s^2 takes values between 0 and 1, where 1 occurs when K = X and hence corresponds to complete success.

It is not hard to prove that

$$\overline{\Delta p_i} = X^T (A^T E^{-1} A + W^{-1})^{-1} A E^{-1} \Delta D \tag{15}$$

and

$$\sigma^2 = X^T (A^T E^{-1} A + W^{-1})^{-1} X \tag{16}$$

are equivalent to (7) and (8), respectively.

INFERRED STRUCTURES AND DISCUSSION

There were several seismic refraction studies in the Tonga-Kermadec-Guam region. Shor et al. (1971) pointed out that crustal thicknesses are about 8-9 km in the Fiji plateau (the north Fiji basin), 6 km in the south Fiji basin, and 14 km in the Fiji islands, and the Tonga, Kermadec, and New Hebrides ridges. Furumoto et al. (1973) indicated that crustal thickness beneath the solomon islands is approximately 13-15 km. The sedimentary layer is about 1.5 km thick and crustal thickness is in the range of 35-42 km, a value of continental type, in the Ontong-Java plateau region (Furumoto et al., 1976). Just a little to the west of the Ontong-Java plateau, crustal thickness shrinks to around 18 km, a value more typical of island arc structures.

Using the earlier surface wave dispersion and body wave refraction studies, Seneff (1978) developed two earth models to fit his Rayleigh wave dispersion data observed in the Tonga-Kermadec-Guam area. His model B has a 2.5 km thick of water layer, 1.5 km thick of sediments, and 23 km thick of crust. The low velocity channel is in the depth range of 77-127 km. We used his model B as our initial model for inversion of the Kermadec-New Britain group data. The starting model for the Tonga group data is modified from this model B by using 3 km water layer instead of 2.5 km. Both of the starting models are relatively simple. The S wave velocities for lithosphere and asthenosphere are 4.46 km/sec and 4.28 km/sec, respectively. The lower velocity channel is at a depth range of about 80-130 km. Because of surface wave dispersion is not very sensitive to P wave velocity and density changes (compare to S wave velocity) and the limitation of the computing facilities our inversion is carried out for shear velocity only.

The inverted shear structure, model KNB, for the propagation path Kermadec-New Britain-Taipei is shown in Figure 8 together with the initial trial model. Table 3 lists the layer shear velocities and corresponding resolution parameters, s^2 and σ^2, as defined in previous section. A comparison between the theoretical and observed data is presented in Figure 6. The overall fit is good, although the agreement at longest period for Rayleigh wave is poor.

It can be seen, from Figure 8, that the final model KNB tends to modify the initial model by causing a decrease in crustal thickness and an increase in the overall shear velocity down to the depth of approximately 380 km. The velocity contrast between anthenosphere and its upper and lower zones remains about the same as the starting model. The better resolved portion for model KNB is the depth range of 4-280 km. The data have little resolution for the parameters below 400km. The thinner crustal thickness, than Seneff's model B (our initial trial model), is not

Table 4.
Layer shear velocities and resolution parameters for model TON

H (km)	β (km/sec)	σ (km/sec)	s^2
3.0	0.000	0.000	0.000
1.5	1.604	0.158	0.019
3.0	3.473	0.105	0.198
5.0	3.834	0.073	0.386
5.0	4.307	0.077	0.278
10.0	4.326	0.051	0.379
10.0	4.617	0.054	0.297
10.0	4.577	0.055	0.287
15.0	4.596	0.043	0.360
15.0	4.623	0.045	0.267
15.0	4.373	0.045	0.250
15.0	4.339	0.046	0.213
20.0	4.323	0.040	0.237
30.0	4.567	0.032	0.253
40.0	4.582	0.028	0.270
40.0	4.585	0.029	0.201
40.0	4.561	0.030	0.132
50.0	4.517	0.027	0.094
50.0	4.471	0.027	0.056
50.0	5.380	0.028	0.020
100.0	5.377	0.019	0.029
100.0	5.384	0.019	0.016
150.00	5.894	0.016	0.006
∞	6.380	—	—

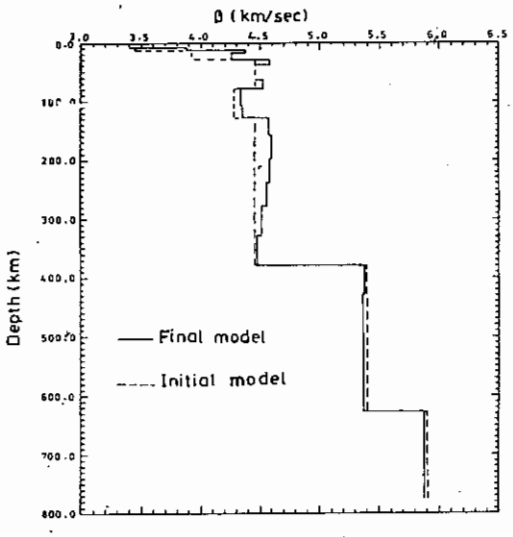

Figure 8. Layer shear velocities for the Kermadec-New Britain-Taipei model KNB compared to the initial trial model.

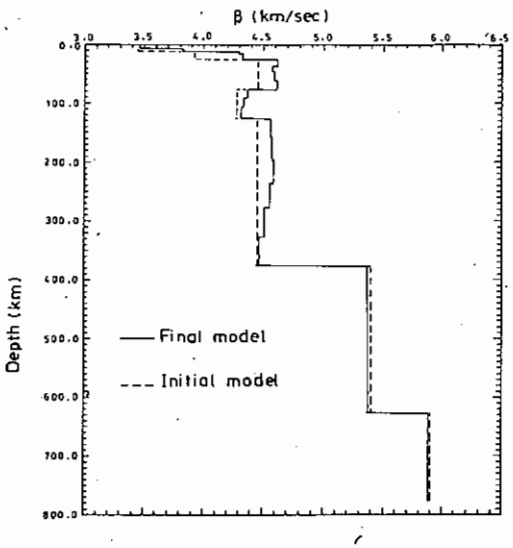

Figure 9. Layer shear velocities for the Tonga-Taipei model TON compared to the initial trial model.

surprising since part of the path Kermadec-New Britain-Taipei is within the Philippine Sea, where crustal thickness is about 6 km (Seekins and Teng, 1977; Yu et al., 1980). The model KNB is an average feature for all the paths.

The final model, TON, that fits the observed dispersion for the path Tonga-Taipei is plotted in Figure 9. The trial starting model is also plotted for comparison. Figure 7 shows the theoretical dispersion curves for the fitted model and the data. The overall fit is about the same as in previous case.

Our final model TON has thinner crust and higher shear velocities for the depth range of 3.0-380 km than the trial model (modified from Seneff's model B). The thinner crust than the results revealed by the refraction studies (Shor et al., 1971, Furumoto et al., 1973, 1976) is also due to the averaging effect for the long propagation path of surface waves.

The best-resolved shear structure for model TON is in the depth range of 4.5-280 km. The resolution for the 400-km and 600-km discontinuities are limited. Table 4 lists the layer velocities and their corresponding resolution parameters. Comparing Figures 8 and 9 and Tables 3 and 4, we can see that both the models KNB and TON have a low velocity channel at about the same depth and velocity, with high resolution. The main differences for this two models are at shallow depth. Model TON has higher shear velocity in the depth range of about 20-75 km.

SUMMARY

The display-equalized filtering technique was used to measure group velocities for both Rayleigh and Love waves in the southwest Pacific region. The 26 earthquakes selected were located in the vicinity of the Tonga, Kermadec and New Britain islands. The propagation paths of these events can be divided into two sets: (1) Tonga-Taipei, and (2) Kermadec-New Britain-Taipei. The Tonga-Taipei path is along the southwest margin of the Pacific and across the south Philippine Sea. The Kermadec-New Britain-Taipei path is confined in the boundary area of the Pacific and Australian plates and the south Philippine Sea plate. The resulting dispersion data were then grouped and inverted using extended Backus-Gilbert inversion method. The inverted regional structures show only some differences in the depth range of approximately 20-75 km.

ACKNOWLEDGEMENTS

The authors would like to thank Drs. G.K. Yu and T.L. Teng for valuable suggestions. This research was supported by National science council by grant no. NSC70-0202-M001-05.

REFERENCES

Dziewonski, A., S. Booch, and M. Landisman (1969). A technique for the analysis of transient seismic signals, *Bull. Seism. Soc. Am., 59,* 427-444.

Franklin, J.N. (1970). Well-posed stochastic extensions of ill-posed linear problems, *Jour. Math. Anal. Appl., 31,* 682-716.

Furumoto, A.S., W.A. Wiebenga, J.P. Webb, and G.H. Sutton (1973). Crustral structure of the Hawaiian Archipelage, northern Melanesia, and the central Pacific basin by seismic refraction methods, *Tectonophysics,* 20, 153-164.

Furumoto, A.S., J.P. Webb, M.E. Odegard, and D.M. Hussong (1976). Seismic studies on the Ontong Java Plateau, 1970, *Tectonophysics,* 34, 71-91.

Gupta, H.K. and K. Hamada (1975). Rayleigh- and Love-wave dispersion up to 140-second-period range in the Indonesia-Philippine region, *Bull. Seism. Soc. Am.,* 65, 507-524.

Isacks, B., J. Oliver, and L. Sykes (1968). Seismology and the New Global Tectonics, *J. Geophys. Res.,* 73, 18, 5855-5899.

Johnson, T. and P. Molnar (1972). Focal mechanisms and plate tectonics of the southwest Pacific, *J. Geophys. Res.,* 77, 5000-5032.

Jordan, T.H. (1973). Estimation of the radial variation of seismic velocities and density in the earth, *Ph.D. Thesis,* Cal. Inst. Tech., Pasadena, Calif. 199 p.

Karig, D.E. (1970). Ridges and basins of the Tonga Kermadec Island Arc system, *J. Geophys. Res., 75,* 239-254.

Karig, D.E. (1971a). Structural history of the Mariana Island Arc system, *Bull. Geol. Soc. Am.,* 82, 323-344.

Karig, D.E. (1971b). Origin and development of marginal basins in the western Pacific, *J. Geophys. Res.,* 76, 2524-2561.

Kuo, J., J. Brune, and M. Major (1962). Rayleigh-wave dispersion in the Pacific Ocean for the period range 24 to 140 seconds, *Bull. Seism. Soc. Am.,* 52, 333-357.

Lin, M.T. and Y.B. Tsai (1981). Seismotectonics in Taiwan-Luzon area, *Bull. Inst. Earth Sci.,* Academia Sinica, this issue.

McCowan, D.W. and R.T. Lacoss (1978). Transfer functions for the seismic research observatory seismograph system, *Bull. Seism. Soc. Am., 68,* 501-512.

Nyman, D.C. and M. Landisman (1977). The display-equalized filter for frequency-time analysis, *Bull. Seism. Soc. Am., 67,* 393-404.

Rodi, W.L. (1975). Unpublished research note.

Santo, T. and Y. Sato (1966). Worldwide survey of the regional characteristics of group velocity dispersion of Ravleigh waves, *Bull. Earthquake Res. Inst.,* Tokyo Univ., 44, 939-964.

Savage, J.C. and W.R. H. white (1969). A map of Rayleigh-wave dispersion in the Pacific, *Can. J. Earth Sci.,* 6, 1289-1300.

Seekins, L.C.and T.L. Teng (1977). Lateral variations in the structure of the Philippine Sea plate, *J. Geophys. Res., 82,* 317-323.

Seneff, S. (1978). A fast new method for frequency-filter analysis of surface waves: application in the west Pacific, *Bull. Seism. Soc. Am.,* 68, 1031-1048.

Seno, T. (1977). The instantaneous rotation vector of the Philippine Sea plate relative to the Eurasian plate, *Tectonophysics, 42,* 209-226.

Shor, G.G., H.K. Kirk, and H.W. Menard (1971). Crustal structure of the Melanesian area, *J. Geophys. Res.,* 76, 2562-2586.

Yeh, Y.T. (1979). A new surface-wave inversion method for determining lateral variations in crust-mantle structure with application to China, *Ph.D Thesis*, The Penn. State Univ., 230 p.

Yu, G.K., Y.T. Yeh and T.C. Shin (1980). Seismic surface wave dispersion in the Ryukyu-Taiwan-Philippine Region and its surrounding Seas, *Bull. Inst. Geophys.* NCU, Taiwan, 20, 52-63.

Institute of Earth Sciences
Academia Sinica
P. O. Box 23-59
Taipei Taiwan
Republic of China
(Y.T.Y.)

Institute of Geophysics
National Central University
Chung Li, Taiwan
Republic of China
(K.C.C.)

西南太平洋區之表面波頻散與地殼—地函構造

葉 永 田　陳 國 誠

摘　　要

本文利用等量化展示濾波法處理，位於東加、新不列顛和克馬得地區的２６個地震，測取其雷利波和樂夫波之群速頻散。這些地震的波傳路徑可分成二類：①東加至台北；②克馬得和新不列顛至台北。測得之頻散曲綫據此分為二組，並利用貝克—基爾博逆推法推求此二測綫下之地殼—地函構造。所得二測綫之構造僅在淺於７５公里之部份有些差異